Triplet-State Conformational Changes in 15-*cis*-Spheroidene Bound to the Reaction Center from *Rhodobacter sphaeroides* 2.4.1 as Revealed by Time-Resolved EPR Spectroscopy: Strengthened Hypothetical Mechanism of Triplet-Energy Dissipation†

Yoshinori Kakitani,‡ Ritsuko Fujii,‡,§ Yasushi Koyama,*,‡ Hiroyoshi Nagae,|| Lee Walker,⊥ Bruce Salter,⊥ and Alexander Angerhofer⊥

Faculty of Science and Technology, Kwansei Gakuin University, Gakuen, Sanda 669-1337, Japan, Kobe City University of Foreign Studies, Gakuen-Higashimachi, Nishi-ku, Kobe 651-2187, Japan, and Department of Chemistry, The University of Florida, Gainesville, Florida 32611-7200

Received June 15, 2005; Revised Manuscript Received December 27, 2005

ABSTRACT: Time-resolved EPR spectra of 15-*cis*-spheroidene bound to the reaction center from *Rhodobacter sphaeroides* 2.4.1 were recorded at low temperatures. (1) A three-component analysis of the spectral-data matrices by singular-value decomposition followed by global fitting identified the transformation of the triplet carotenoid, ^{3}Car(I) → ^{3}Car(II); during this process, the leak of the triplet population was suggested. A four-component analysis suggested the presence of a representative intermediate, ^{3}Car(R), that forms a leak channel of the triplet population. (2) A theoretical calculation of the zero-field splitting parameters, $|D|$ and $|E|$, by the use of a polyene model, showed that the transformation, ^{3}Car(I) → ^{3}Car(R) → ^{3}Car-(II), accompanies the conformational changes of (0°, 0°, 0°) → (+20°, −20°, +20°) → (+45°, −40°, +40°) around the central *cis* C15═C15′, *trans* C13═C14, and *trans* C11═C12 bonds, respectively. (3) The initial, rapid decrease followed by the inversion of spin polarization along the *z* axis of ^{3}Car was observed, which was correlated with a change in the spin angular momentum. (4) In reference to the binding pocket of the Car, determined by X-ray crystallography, the conformational changes were ascribed to the intrinsic isomerization property of 15-*cis* ^{3}Car as well as the Car−peptide intermolecular interaction; a detailed picture was proposed. All of the above results support the mechanism of triplet-energy dissipation proposed previously: the rotational motions around the central double bonds cause a change in the orbital angular momentum and, through the spin−orbit coupling, a change in the spin angular momentum, which enhances the T_1 → S_0 intersystem crossing dissipating the triplet energy.

The major function of carotenoids (Cars)[1] in photosynthetic reaction centers (RCs) can be regarded as photoprotection, which primarily includes the quenching of the triplet state of the special-pair bacteriochlorophyll (^{3}P) followed by the dissipation of triplet energy (*1*). Under the reducing conditions, this function becomes crucial because the reverse electron transfer and the charge recombination can take place to form ^{3}P, which sensitizes the generation of harmful singlet oxygen.

A unique *cis* configuration of the Car in the RC from a purple bacterium was discovered by Lutz et al. (*2*), and the 15-*cis* configuration was proposed by Koyama et al. (*3*, *4*), both by means of Raman spectroscopy. The 15-*cis* configuration of the RC-bound Car was also proposed by electronic-absorption, circular dichroism (CD), and solid-state ^{13}C nuclear magnetic resonance (NMR) spectroscopies (see ref *5* for a review). Direct evidence for the 15-*cis* configuration was given by ^{1}H NMR spectroscopy of Cars extracted from the RCs, first for spheroidene (*6*) and then for neurosporene (*7*) and spirilloxanthin (*8*).

To reveal the reason for the selection of the 15-*cis* configuration by the RC-bound Car for the photoprotective function, the T_1 (the lowest triplet)-state properties of the *cis*−*trans* isomers of Cars in solution were examined. (a) With *β-carotene*, upon triplet excitation, the 15-*cis* isomer gave rise to exactly the same transient-Raman (*9*) and transient-absorption (*10*) spectra as those of the all-*trans* isomer, although the 7-*cis*, 9-*cis*, and 13-*cis* isomers exhibited their own unique spectral patterns in the T_1 state. The

† This work has been supported by a Grant "Open Research Center Project" from the Ministry of Education, Culture, Sports, Science, and Technology, Japan, an International Joint Research Grant from New Energy and Industrial Technology Development Organization (NEDO), Japan (to Y.K.), a Grant-in-Aid, 15770100, from the Ministry of Education, Culture, Sports, Science, and Technology, Japan (to R.F.), and a Grant from the National Science Foundation, MCB-9977452, U.S.A. (to A.A.).

* To whom correspondence should be addressed. Telephone and Fax: +81-79-565-8408. E-mail: ykoyama@kwansei.ac.jp.

‡ Kwansei Gakuin University.

§ Current address: Department of Physics, Graduate School of Science, Osaka City University, Sugimoto, Sumiyoshi-ku, Osaka 558-8585, Japan.

|| Kobe City University of Foreign Studies.

⊥ The University of Florida.

[1] Abbreviations: B_M, accessory bacteriochlorophyll bound to the M subunit; Car, carotenoid; CD, circular dichroism; EPR, electron paramagnetic resonance; H_M, bacteriopheophytin bound to the M subunit; LH2, light-harvesting complex 2; NMR, nuclear magnetic resonance; P, special-pair bacteriochlorophyll; Q_B, quinone bound to the M subunit; RC, reaction center; *Rba.*, *Rhodobacter*; S_0, ground state; SAS, species-associated spectra; SLR, spin-lattice relaxation; SVD, singular-value decomposition; T_1, lowest triplet state.

10.1021/bi0511538 CCC: $33.50
Published on Web 01/28/2006

quantum yields of triplet-sensitized isomerization were in the order, 7-*cis* (0.12) < 9-*cis* (0.15) ≪ 13-*cis* (0.87) < 15-*cis* (0.98) (*11*). (b) For *spheroidene* (*12*), (1) the lifetime of *cis* T_1 (0.83 μs) was much shorter than that of all-*trans* T_1 (4.76 μs), clearly indicating the advantage of the *cis* isomers in the triplet-energy dissipation. (2) The time constants of *cis*−*trans* isomerization in the T_1 state followed the order, 15-*cis* (0.56 μs) < 13-*cis* (0.77 μs) < 9-*cis* (0.83 μs) < 13′-*cis* (0.91 μs), and the ranking of the quantum yield of triplet-sensitized isomerization was 15-*cis* (0.60) > 13-*cis* (0.52) > 9-*cis* (0.50) > 13′-*cis* (0.48). (3) Most importantly, the time constants of *cis*−*trans* isomerization for the *cis* isomers (0.56−0.91 μs) were similar to that of $T_1 \rightarrow S_0$ (ground state) intersystem crossing (0.83 μs), a fact that suggests that the rotational motion around the *cis* C15═C15′ bond triggers the $T_1 \rightarrow S_0$ relaxation. Thus, the 15-*cis* isomer is unique in its capability for "rapid isomerization toward all-*trans*" after excitation to its T_1 state. This can be rationalized by the steric hindrance in the 15-*cis* bent structure and by a decrease in the bond order of the central double bonds in "the triplet-excited region" (*11*, *13*).

The T_1-state structure of spheroidene bound to the RC was examined by transient-Raman spectroscopy: (a) a pioneering work by Lutz and co-workers showed that the RC-bound Cars, spheroidene and methoxyneurosporene, retained the 15-*cis* configuration that was strained (*14*). (b) Subsequent T_1 Raman spectroscopy of the RC from *Rhodobacter* (*Rba.*) *sphaeroides* 2.4.1 showed a large decrease in the bond order and a substantial twisting of the central double bond(s) of the conjugated chain (*15*). (c) The structure of the RC-bound T_1 spheroidene was examined by normal-coordinate analysis of the Raman spectra of the undeuterated and six differently deuterated spheroidenes that were incorporated into the carotenoidless RC from *Rba. sphaeroides* R26 (*16*). The set of T_1-state carbon−carbon stretching force constants that were determined for the RC-bound 15-*cis*-spheroidene was similar to that determined for all-*trans*-spheroidene free in solution. Changes in those stretching force constants, upon triplet excitation, clearly showed a decrease (increase) in the bond order of the C═C (C−C) bonds in the central part of the conjugated chain, enhancing the 15-*cis* to all-*trans* isomerization. Concerning the conformation of the conjugated backbone of the RC-bound spheroidene in the T_1 state, the torsional angles around the *cis* C15═C15′, *trans* C13═C14, and *trans* C11═C12 bonds were proposed to be +45°, −30°, and +30°, respectively.

To examine such a large conformational change in the T_1 state of the RC-bound spheroidene, time-resolved electron paramagnetic resonance (EPR) spectroscopy is expected to be most powerful, because it can directly probe the T_1 species: (a) the first time-resolved EPR experiment on the Car triplet state (^{3}Car) was reported by McGann and Frank (*17*). These workers obtained the sublevel decay rates of the spheroidene triplet state in reduced chromatophores of *Rba. sphaeroides* using a model of a single ^{3}Car without allowing for conformational changes. The observed rates were of the order of $0.9-4 \times 10^5$ s^{-1} with the spin-lattice relaxation (SLR) rates an order of magnitude slower. (b) Most recently, Borovykh et al. (*18*) studied triplet 15-*cis*-spheroidene in the RC from *Rba. sphaeroides* 2.4.1 by time-resolved, direct-detection EPR spectroscopy upon excitation with polarized light. They determined the orientation of the transition dipole moments of spheroidene and the special pair (P) relative to the triplet principal axes.

In the present investigation, we have attempted to examine the T_1 state of the RC-bound 15-*cis*-spheroidene by means of time-resolved EPR spectroscopy, at low temperatures, hoping to identify its conformational changes. We have addressed the following three specific questions: (1) Is there experimental evidence, apart from resonance Raman spectroscopy, for the above-mentioned conformational change in the T_1 state, i.e., from the ground-state conformation immediately after excitation to the substantially twisted conformation? (2) Can the $T_1 \rightarrow S_0$ intersystem crossing channel that dissipates the triplet energy (population) be identified during the conformational change? (3) Can the predicted change in the spin angular momentum be detected during the conformational change?

These questions were based on the hypothetical mechanism of triplet-energy dissipation by the RC-bound Car proposed previously (*12*, *15*, *16*), the details of which will be described later.

MATERIALS AND METHODS

Sample Preparation and EPR Spectroscopy. The RC from *Rba. sphaeroides* 2.4.1 was prepared as described previously (*15*). Approximately 50 mM of sodium dithionite was added to a concentrated sample suspension containing 40−60% glycerol ($OD_{800} = \sim 150$ cm^{-1}). The details of the experimental conditions are described in the Supporting Information (page 2′). Time-resolved EPR spectra were recorded at 55−145 K after excitation of 15-*cis*-spheroidene by 532 nm (~6 ns and 30 Hz) pulses from a Nd:YAG laser, whose electric vector was perpendicular to the magnetic field ($E \perp B_0$). Time-resolved EPR spectra were taken with a commercial Bruker Elexsys E580 pulse/cw spectrometer equipped with a 3 mm ID split ring resonator (Bruker Flexline). The experiment employed Bruker's SpecJet transient digitizer to record the spectra. They were obtained in "direct detection mode" without field modulation. This means that the microwaves are constantly on. Detection of the transients induced by the laser starts approximately 600 ns before the flash. The transient oscilloscope (Bruker SpecJet) was triggered by the laser trigger. The phase was adjusted manually for optimal detection at each temperature point. The experiment is conceptually the same as described originally by Kim and Weissman (*19*). Microwave power was set to 30 dB (0.2 mW) to avoid artifacts in the transient decay from Torrey oscillations (*20*). To further reduce instrumental noise, the AFC was switched off after the instrument had warmed and was running stable at a fixed frequency. Transients were averaged at the laser repetition rate of 30 Hz until a sufficiently good signal-to-noise ratio was obtained. This meant that each transient in the 2D spectra consisted of a sum from 16 to 60 individual transients (the higher number was necessary at higher temperatures). Additional information is given in the Supporting Information (page 2′).

The EPR data matrices with a dimension of 101 × 333 data points, in the 3050−3850 G magnetic-field region (with an interval of 8 G) and the (−0.6) − 16 μs time region (with an interval of 0.05 μs), were analyzed by singular-value decomposition (SVD) followed by global fitting (*21*−*23*).

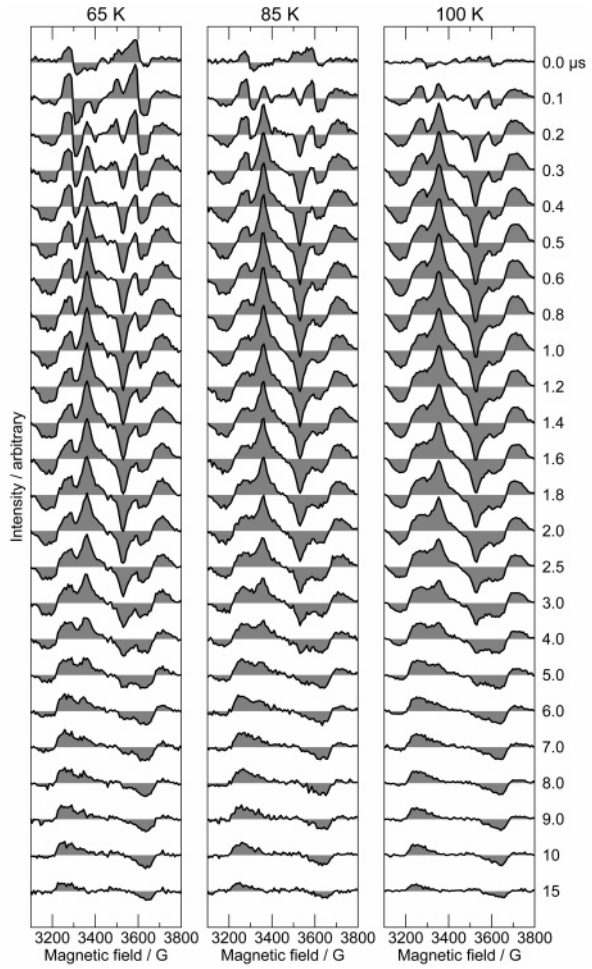

FIGURE 1: Submicrosecond time-resolved EPR spectra of the RC from *Rba. sphaeroides* 2.4.1 (recorded at 65, 85, and 100 K) after excitation of spheroidene by the use of the 532 nm pulses whose electric vector was perpendicular to the magnetic field ($E \perp B_0$). Representative spectra are selected from each data matrix.

Calculation of the zero-field splitting parameters and simulation of spectral patterns are described in the Supporting Information (pages 2′−4′).

RESULTS

A Set of ^{3}Car Species Identified in the Time-Resolved EPR Spectra: (a) Two ^{3}Car Species Identified by Inspection of the Raw Time-Resolved Spectra. Figure 1 shows the submicrosecond time-resolved EPR spectra of the RC from *Rba. sphaeroides* 2.4.1 (at 65, 85, and 100 K). First, we focus our attention to the time-resolved spectra at 65 K, in which three major components are most clearly seen: the spectrum immediately after excitation (delay time 0.1 μs, for example) can be assigned to ^{3}P by referring to the EPR spectrum of the RC from *Rba. sphaeroides* R26 (a carotenoidless mutant) that was recorded by Borovykh et al. (*24*). The spectrum after the decay of the ^{3}P signal (1.4 μs after excitation) can be assigned to a triplet state of Car, which we call "^{3}Car(I)". The spectral pattern appearing at later stages (10 μs) can also be assigned to a triplet state of Car, which we call "^{3}Car(II)". Thus, the above spectral changes can be ascribed to a sequential transformation of $^3\text{P} \rightarrow {}^3\text{Car(I)} \rightarrow {}^3\text{Car(II)}$. On going to higher temperatures (85 and 100 K), the initial contribution of the ^{3}P signal decreases, but the ^{3}Car(I) → ^{3}Car(II) transformation remains almost unaffected. (The reason those different triplet species were *not* identified in the previous investigation is discussed in the Supporting Information (page 4′).)

Table 1: Transformation and Decay Time Constants (in Microseconds) Defined for the Dynamic Schemes Shown Below[a,b]

temperature	k_1^{-1}	k_2^{-1}	k_3^{-1}	k_4^{-1}	k_5^{-1}	$(k_4 + k_5)^{-1}$
65 K	0.47	3.97	9.69	∼2.0	∼1.0	∼0.67
85 K	0.33	3.59	9.19	∼2.0	∼1.0	∼0.67
100 K	0.31	3.37	8.47	∼2.0	∼1.0	∼0.67

[a] Three-component analysis:

$$^3\text{P} \xrightarrow[k_1]{} {}^3\text{Car(I)} \xrightarrow[k_2]{} {}^3\text{Car(II)} \quad (k_3)$$

[b] Four-component analysis:

$$^3\text{P} \xrightarrow[k_1]{} {}^3\text{Car(I)} \xrightarrow[k_2]{} {}^3\text{Car(R)} \xrightarrow[k_4]{} {}^3\text{Car(II)}$$
$$(k_5) \qquad (k_3)$$

(b) Two ^{3}Car Species Confirmed by a Three-Component SVD and Global-Fitting Analysis. To determine the spectral pattern and the decay time constant of each component, we performed SVD followed by global fitting of the time-resolved spectral data (at 65, 85, and 100 K) by the use of a three-component model (the scheme is shown in Table 1). The negligible contribution of SLR (*18*) facilitated the SVD and global-fitting analysis. Figure 2a shows the results at 100 K, including the species-associated spectra (SAS, the top panels) and the time-dependent changes in the population (the bottom two layers of panels in different time scales). The SAS patterns of the three components were basically the same among different temperatures, although the SAS of ^{3}Car(I) at 65 K contained some contribution of ^{3}P (data not shown). Table 1 lists the time constants relevant to ^{3}P, ^{3}Car(I), and ^{3}Car(II).

We have tried to determine the barriers for the transformations, $^3\text{P} \rightarrow {}^3\text{Car(I)} \rightarrow {}^3\text{Car(II)}$, by the use of the sequential model (see Table 1). Figure S1 in the Supporting Information (page 5′) shows an Arrhenius plot. The results can be summarized as follows: (i) the barrier to the P → Car triplet-energy transfer was determined to be 99 ± 5 cm^{-1} (hereafter, approximated by ∼100 cm^{-1}) in agreement with the values previously determined by time-resolved absorption spectroscopy, i.e., 140 ± 100 cm^{-1} (*25*) and 95 ± 10 cm^{-1} (*26*). This barrier has been ascribed to the energy for excitation to the intermediate, the accessory bacteriochlorophyll bound to the M subunit (B_M), in the $\text{P} \rightarrow \text{B}_\text{M} \rightarrow$ Car triplet-energy transfer. The numbers given should be taken as an average activation energy because of the inherent heterogeneity of the triplet energy levels in the sample (*26*). (ii) The barrier to the $^3\text{Car(I)} \rightarrow {}^3\text{Car(II)}$ transformation was determined to be 15 ± 5 cm^{-1} (∼15 cm^{-1}). (iii) The barrier for the decay of ^{3}Car(II) to the S_0 state, determined to be 21 ± 5 cm^{-1} (∼20 cm^{-1}), is also very small and the same as that for the $^3\text{Car(I)} \rightarrow {}^3\text{Car(II)}$ transformation within experimental error. This barrier is very small and not much different from what has been observed by transient optical spectroscopy (32 ± 2 cm^{-1}) for the $^3\text{Car} \rightarrow {}^1\text{Car}$ (ground state) relaxation (*26*).

(c) A ^{3}Car Intermediate Suggested by a Four-Component SVD and Global-Fitting Analysis. The singular values obtained by SVD were $V_1 = 17.4$, $V_2 = 6.8$, $V_3 = 1.2$, $V_4 = 0.5$, and $V_5 - V_{18} = 0.2$; the difference between V_4 and the

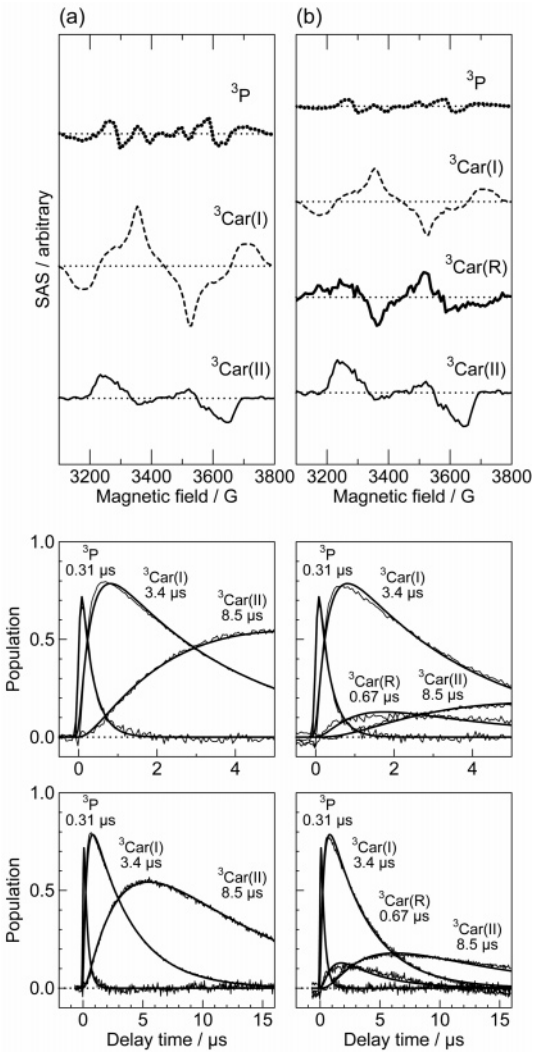

FIGURE 2: Results of SVD followed by global fitting of time-resolved EPR spectra at 100 K by (a) the three-component analysis and (b) the four-component analysis using schemes shown in Table 1. The SAS and the time-dependent changes in the population are shown; in the latter, each set of thinner noisy line and thicker smooth line indicates the time profiles derived from the data and the results of fitting.

noise components V_5-V_{18} justified to proceed to a four-component analysis incorporating a particular intermediate. Table 1 also presents the scheme for the four-component analysis, in which a leakage channel from what we call "^{3}Car(R)" is explicitly incorporated. In the four-component analysis at 65, 85, and 100 K, the decay time constants relevant to ^{3}P, ^{3}Car(I), and ^{3}Car(II) that had been determined by the three-component analysis were transferred, and only the time constants of the ^{3}Car(R) → ^{3}Car(II) transformation and the ^{3}Car(R) decay were adjusted by manual fitting to be about 2.0 and 1.0 μs, respectively (see Table 1). Figure 2b shows the results of the four-component analysis (at 100 K), including the SAS and the time-dependent changes in the population for ^{3}P, ^{3}Car(I), ^{3}Car(R), and ^{3}Car(II).

Conformations of ^{3}Car(II) and ^{3}Car(R) as Determined by the Zero-Field Splitting Parameters: (a) Spectroscopic Determination of the Zero-Field Splitting Parameters, |D| and |E|. Figure S2 in the Supporting Information (page 5′) reproduces the SAS of ^{3}Car(I), ^{3}Car(R), and ^{3}Car(II) determined at 100 K (Figure 2b). Table 2a lists the zero-field splitting parameters determined by those spectral patterns. On going from ^{3}Car(I) to ^{3}Car(II), the $|D|$ value decreases to $\sim^3/_4$ of its original value, whereas the $|E|$ value is reduced by $\sim^1/_2$, in both the three- and four-component analyses. On going from ^{3}Car(I) to ^{3}Car(R), both the $|D|$ and $|E|$ values decrease to $\sim^9/_{10}$ of their original value as determined by the four-component analysis.

Table 2: Zero-Field Splitting Parameters, $|D|$ and $|E|$ (in 10^{-4} cm^{-1}), (a) Determined for the RC-Bound 15-*cis*-Spheroidene for ^{3}Car(I), ^{3}Car(II), and ^{3}Car(R), (b) Calculated for the Polyene Model Using a Flat Conjugated Chain, and (c) Calculated for the Polyene Models Using a Slightly Twisted Conjugated Chain Determined by X-ray Crystallography (*27*)

	^{3}Car(I)	^{3}Car(II)	^{3}Car(R)
(a)			
$\|D\|$	290 (1)	213 (0.73)	262 (0.90)
$\|E\|$	44 (1)	22 (0.50)	39 (0.89)
(b)	(0°, 0°, 0°)	(+45°, −40°, +40°)	(+20°, −20°, +20°)
$\|D\|$	289 (1)	238 (0.82)	283 (0.98)
$\|E\|$	62 (1)	31 (0.50)	55 (0.89)
(c)	(−4°, −2°, −2°)	(+46°, −47°, +43°)	(+21°, −27°, +23°)
$\|D\|$	291 (1)	262 (0.90)	297 (1.02)
$\|E\|$	64 (1)	35 (0.55)	59 (0.92)

(b) Calculation of the Zero-Field Splitting Parameters by the Use of Polyene Models. Table 2b lists the values of the zero-field splitting parameters, $|D|$ and $|E|$, that were calculated for a set of polyene models in different conformations. On the basis of the results of X-ray crystallography (PDB entry 1YST, *27*), we assumed a flat conformation (0°, 0°, 0°) with the torsional angles around *cis* C15═C15′, *trans* C13═C14, and *trans* C11═C12, for ^{3}Car(I) that is directly populated through the triplet-energy transfer from ^{3}P; a pair of flat all-*trans* conformations was assumed on both sides of the 15-*cis* bend as well. To explain the $|D|$ and $|E|$ values in ^{3}Car(II), we first used a model with the three torsional angles set to (+45°, −30°, +30°), which was determined previously based on the normal-coordinate analysis of the T_1 Raman spectra (*16*). On going from the flat (0°, 0°, 0°) to this conformation, the predicted $|D|$ and $|E|$ values decreased to 89 and 65%, respectively. We further refined the model by systematically changing the torsional angles around the three double bonds by 5° in both directions. The resultant model realized the reduction of $|D|$ and $|E|$ to 82 and 50%, in a much better agreement with the observed reduction of 73 and 50%. This result indicates that ^{3}Car(II) represents a strongly twisted conformation with torsional angles (+45°, −40°, +40°) around the *cis* C15═C15′, *trans* C13═C14, and *trans* C11═C12 bonds, respectively.

Table 2b also lists the $|D|$ and $|E|$ values for a model of ^{3}Car(R) having a set of more relaxed torsional angles (+20°, −20°, +20°), somewhat between the (0°, 0°, 0°) and (+45°, −40°, +40°) conformations of ^{3}Car(I) and ^{3}Car(II). The predicted decrease in the $|D|$ and $|E|$ values when comparing this relaxed configuration with the flat one, i.e., 98 and 89%, is fairly small and in rough agreement with those observed, i.e., 90 and 89%, respectively. The calculated $|D|$ values tend to be higher than the observed values in both models of ^{3}Car(II) (82 versus 73%) and ^{3}Car(R) (98 versus 90%) for some reason. Because $|E|$ is a measure of the asymmetry of the triplet state wave function in the *x*,*y* plane, which is roughly perpendicular to the long molecular axis (see Figure 3), it should be more sensitive to the expected twisting motion. The predicted changes in $|E|$ fit very well to those

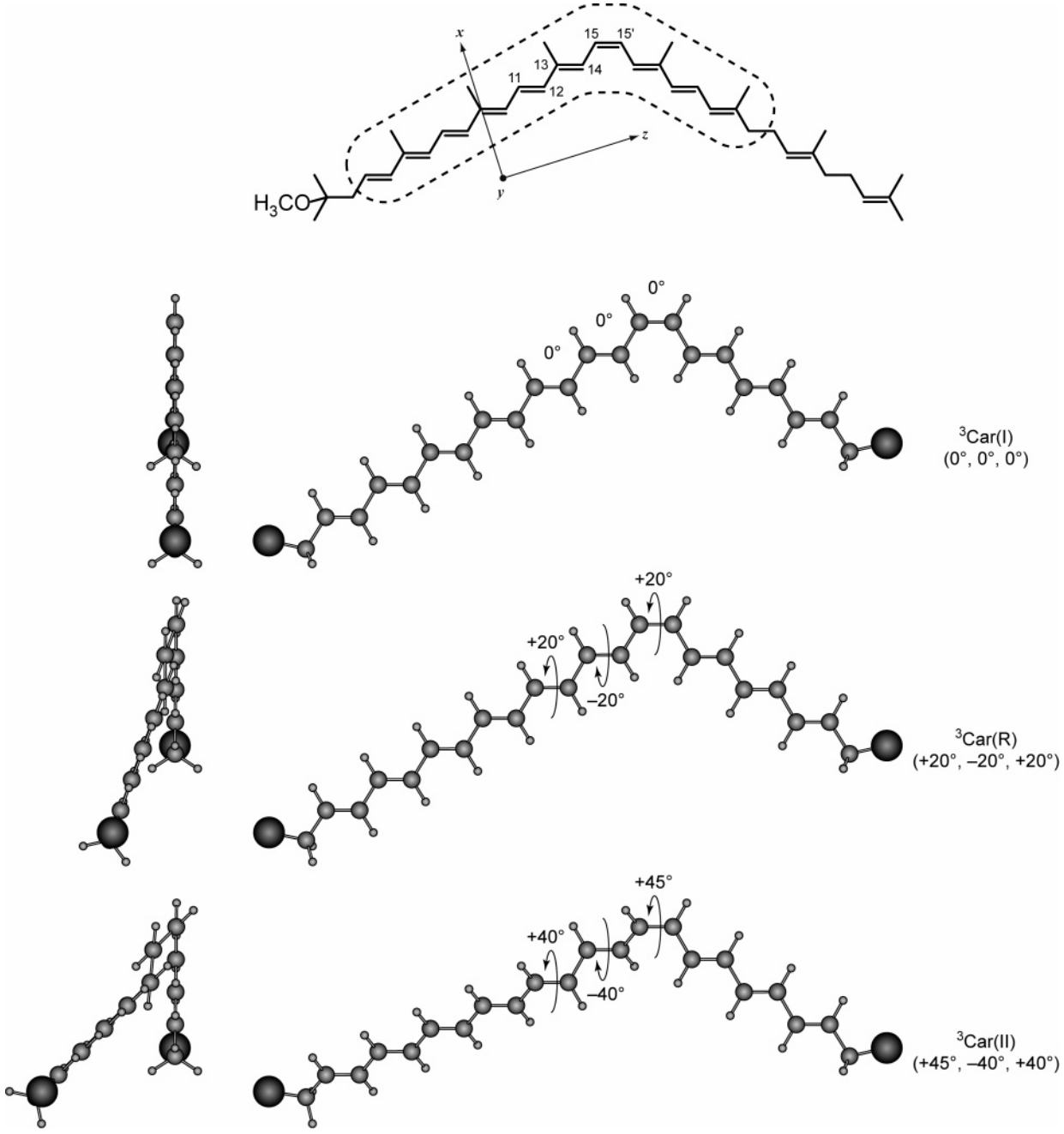

FIGURE 3: Chemical structure of 15-*cis*-spheroidene with the triplet principal axes (the top), and a set of polyene models for ^{3}Car(I), ^{3}Car(R), and ^{3}Car(II) (the bottom three), whose torsional angles around the *cis* C15═C15′, *trans* C13═C14, and *trans* C11═C12 bonds are (0°, 0°, 0°), (+20°, −20°, +20°), and (+45°, −40°, +40°), respectively. The nonconjugated peripheral parts at both ends are truncated and shown by balls.

derived from the experiment. On the basis of these calculations, we conclude that ^{3}Car(R) takes a conformation with the torsional angles approximately at (+20°, −20°, +20°) around the *cis* C15═C15′, *trans* C13═C14, and *trans* C11═C12 double bonds.

Figure 3 (the bottom three) depicts the conformations (0°, 0°, 0°), (+20°, −20°, +20°), and (+45°, −40°, +40°) for ^{3}Car(I), ^{3}Car(R), and ^{3}Car(II), respectively.

Time-Dependent Changes in Spin Polarization along the x, y, and z Principal Axes. Each EPR spectrum (SAS) of ^{3}Car(I), ^{3}Car(R), or ^{3}Car(II) originates from the triplet species in all of the spherical orientations. We tried to decompose each entire spectrum into the $x-x'$, $y-y'$, and $z-z'$ components, taking a certain opening angle of a cone around the *x*, *y*, or *z* axis, and to determine the scaling factors with the + or − sign to present the spin polarization. Then, we used those scaling factors, together with the time-dependent changes in the population of the triplet species, to obtain a measure of the time-dependent changes in the spin polarization (see page 7′ of the Supporting Information for details).

The upper panel of Figure 4 shows the time-dependent changes in the spin polarization (the difference in the spin sublevel populations, i.e., $N_0 - N_{+1}$ (N_{-1})) for the $x-x'$, $y-y'$, and $z-z'$ components thus obtained. The time profiles clearly show that the spin polarization varies depending upon the direction of the external magnetic field, i.e., around the *x*, *y*, or *z* axis. The sudden increase in the spin polarization,

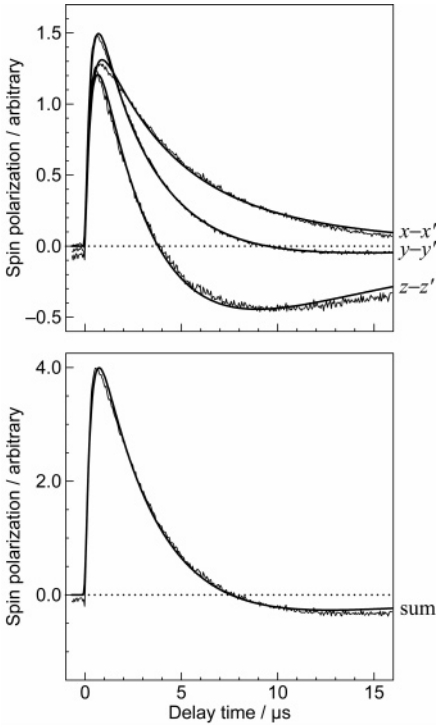

FIGURE 4: Time-dependent changes in the spin polarization for the $x-x'$, $y-y'$, and $z-z'$ components and their sum. The ordinate scale presents the difference in the triplet populations, i.e., $N_0 - N_{+1}$ (N_{-1}). The noisy thinner lines and the smooth thicker lines indicate the time profiles derived from the data and the results of fitting originating from those in Figure 2.

reflecting the population of $N_0 > N_{+1} = N_{-1}$, takes place in all of the orientations immediately after excitation. This rising phase and its observed polarization pattern reflect the triplet-energy transfer from ^{3}P that has been generated by the radical-pair mechanism (*28*). The decay phase of each orientation can be characterized as follows: (i) the $x-x'$ component decays to 0, keeping the same spin polarization; (ii) the $y-y'$ component slightly reverses its spin polarization before reaching 0; and (iii) the $z-z'$ component exhibits rapid decay and inversion of its spin polarization followed by a slow convergence to 0. The lower panel of Figure 4 shows a sum of the three components; the inversion of the overall spin polarization is clearly shown.

This is rather a surprising result. If the triplet-energy transfer takes place from ^{3}P that is generated through the radical-pair mechanism, the initial population on the three spin sublevels should be $N_0 = 1$ and $N_{+1} = N_{-1} = 0$. Then, N_0 should decay to 0 through intersystem crossing, keeping $N_{+1} = N_{-1} = 0$. Then, there is no chance for the spin polarization, $N_0 - N_{+1}$ (N_{-1}), to become negative within an isolated spin system.

The only mechanism to explain the observation that we can think of is the spin−orbit coupling. Now, we notice that the inversion of the spin polarization predominantly takes place along the *z* axis, approximately in the same direction of the C15═C15′, C13═C14, and C11═C12 bonds (see Figure 3), around which the rotational motions take place in the RC-bound Car in the triplet state. Here, the neighboring molecules, including the B_M and the peptide, may function as "a spin and energy reservoir" to facilitate such inversion of spin polarization in the Car molecule.

Because we have found something unique and extraordinary by low-temperature EPR spectroscopy of the RC-bound 15-*cis*-spheroidene in the triplet state, we probably need to prove that our analyses of time-resolved spectra were reliable enough. From this viewpoint, we will describe the details of the analytical procedure and present (as proof) the time-resolved spectra that were reconstituted by the use of the relevant results of analysis to compare with the time-resolved spectra that we actually observed. We will describe the following three cases: (1) the four-component, SVD, and global-fitting analysis, which identified the conformational changes of ^{3}Car(I) → ^{3}Car(R) → ^{3}Car(II) and the leak of the triplet population from the intermediate, ^{3}Car(R); and (2) the time-dependent changes in spin polarization in the $x-x'$, $y-y'$, and $z-z'$ components, which indicated the predominant inversion of spin polarization along the *z* axis. All those findings relied on the analytical technique of SVD followed by global fitting. We also tried to find out what should have happened (3) when we had analyzed the time-resolved spectra without considering the changes in the zero-field splitting parameters, $|D|$ and $|E|$, as well as the inversion of spin polarization. (All those details are presented in the Supporting Information (pages 6′−14′); those readers who may not be interested in this type of particular issues, please proceed directly to the Discussion.)

DISCUSSION

Triplet-State Properties of the RC-Bound 15-cis-Spheroidene as Revealed by Time-Resolved EPR Spectroscopy: (a) Conformational Changes around the Central Double Bonds. The torsional angles around the *cis* C15═C15′, *trans* C13═C14, and *trans* C11═C12 bonds were determined for ^{3}Car(II) and ^{3}Car(R) based on the comparison of the zero-field splitting parameters, $|D|$ and $|E|$, between the experiment and calculations of polyene models in various configurations. Figure 3 depicts the predicted conformations most closely matching the experiment. In the comparison, we used the reduction of those parameters on going from ^{3}Car(I) to ^{3}Car(II) or from ^{3}Car(I) to ^{3}Car(R), taking the flat (0°, 0°, 0°) conformation in ^{3}Car(I) as a reference. We also used the slightly twisted (−4°, −2°, −2°) ground-state conformation as a reference (see Figure S10 in the Supporting Information, page 15′). Table 2 shows the results; the optimum conformation is slightly changed, and the fitting to the reduction of the $|D|$ and $|E|$ values becomes worse. The results suggest that the flat conformation may be more favorable for the triplet species, because the flat all-*trans* conformation is eventually formed upon triplet excitation of free 15-*cis* Cars in solution.

(b) Leak Channel of Triplet Population. Figure 2 compares the results of the three- and four-component analyses (at 100 K) by the use of the schemes shown in Table 1. The fitting between the observed and calculated time-dependent changes in the population (the lower panels) and time-resolved spectra at different delay times (not shown) were almost the same between the three- and four-component analyses. It can be concluded that both schemes are almost equally relevant. In other words, the two different schemes are a pair of different expressions of the same excited-state dynamics that include the leakage of the triplet population during the conformational change from ^{3}Car(I) to ^{3}Car(II). It is to be noted that the SAS of ^{3}Car(II) is much lower in intensity ($^1/_3$) than that

Scheme 1

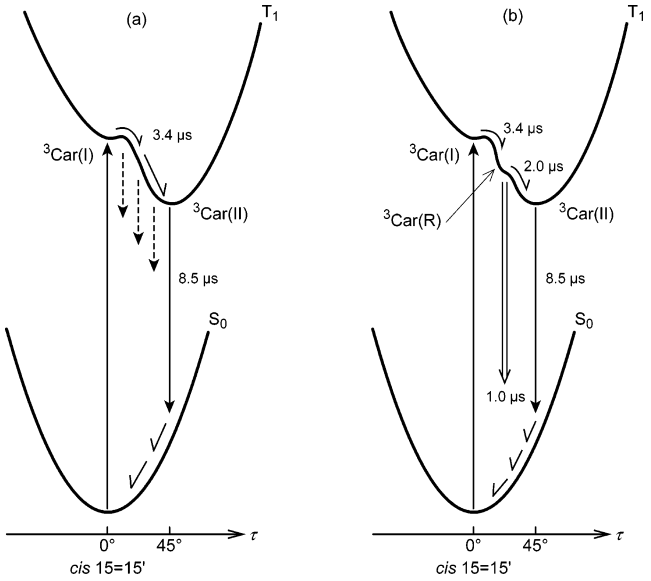

of ^{3}Car(I) in the three-component analysis, whereas their intensities are comparable in the four-component analysis.

Parts a and b of Scheme 1 pictorially compare the triplet-state dynamics expressed in terms of the three- and four-component analyses. In the former, the leakage of the triplet population is implicitly incorporated, and the effect is reflected by the reduced amplitude of the ^{3}Car(II) signal. In the latter, the leakage of the triplet population is explicitly incorporated in the form of ^{3}Car(R), which is a representative intermediate for relaxation. Thus, the pair of fitting results strongly suggests the presence of leakage channel(s) of the triplet population. For this reason, we tend to consider the presence of ^{3}Car(R) as a physically significant reflection of the intermediate potential surface on the way from ^{3}Car(I) to ^{3}Car(II).

The barriers ($\sim$15 cm^{-1}) for the ^{3}Car(I) $\rightarrow$ ^{3}Car(II) transformation, determined in the three-component analysis, may correspond to that of ^{3}Car(I) $\rightarrow$ ^{3}Car(R) transformation in the four-component analysis. The barrier for the subsequent ^{3}Car(R) $\rightarrow$ ^{3}Car(II) transformation should be practically 0, because the time constant of this transformation is temperature-independent (Table 1).

(c) Inversion of Spin Polarization during Conformational Changes. We observed the *rapid decay* and *inversion* of the spin polarization in the *z* orientation, reflecting the changes in the relative population, N_0 versus $N_{+1} = N_{-1}$ (Figure 4). The timing of the population inversion (3.8 μs) is roughly the same as or slightly slower than that of the generation of the ^{3}Car(R) leakage channel (3.4 μs) shown in Scheme 1b. It strongly suggests that the most efficient $T_1 \rightarrow S_0$ intersystem crossing (or in other words, a change in the spin angular momentum from $\mathbf{S} = 1$ to $\mathbf{S} = 0$) is taking place through the depopulation of N_0 along the *z* axis. Further, as mentioned above, the *z* axis of triplet 15-*cis*-spheroidene is approximately parallel to the C15═C15′, C13═C14, and C11═C12 bonds (see the top of Figure 3), around which the rotational motion takes place in the triplet transformation of ^{3}Car(I) $\rightarrow$ ^{3}Car(R) $\rightarrow$ ^{3}Car(II).

There must be some mechanism in which the rotational motion gives rise to the rapid relaxation of the N_0 triplet population along the *z* axis of ^{3}Car. The detailed mechanism of the triplet depopulation is still an open question, although a preliminary calculation showed that the spin−orbit coupling can be strongly enhanced by twisting around the conjugated double bonds. Therefore, it is tempting to correlate the rotational motion to a change in the orbital angular momentum.

We have conducted preliminary time-resolved EPR spectroscopy of the light-harvesting complex 2 (LH2) from *Rba. sphaeroides* 2.4.1 at 85 K, the results of which are contrasted to the present case of the RC in the Supporting Information (page 15′). No signs of conformational changes or the inversion of spin polarization were found in all-*trans*-spheroidene in the antenna complex.

Conformational Changes of ^{3}Car in the Binding Pocket of the RC Determined by X-ray Crystallography: (a) Structural Characteristics of 15-cis-Spheroidene and the Binding Pocket of the RC. Figure 5a shows the binding pocket that have been determined by X-ray crystallography (PDB entry 1YST, *27*). (The surrounding atoms within a distance of 10 Å from the Car skeleton are presented.) Concerning the steric interaction between the binding pocket and the conjugated chains of Car, on both sides of the 15-*cis* bend, the shorter conjugated side (the right-hand side in Figure 3) is tightly fixed by the amino acid side chains of the apopeptide, whereas the longer conjugated side (the left-hand side) is in "an open space" of the X-ray structure. (It is to be noted that the longer conjugated side is on the left-hand side in Figure 5a and on the right-hand side in Figure 5b.) "The open space" is not a real open space but probably a region, where the hydrocarbon side chains of the peptide, B_M, bacteriopheophytin (H_M), and quinone (Q_B) are packed in irregular conformations. Presumably, no atoms could be specifically located in this particular region in the modeling process by the use of an electron-density map of a 3.0 Å resolution in this particular X-ray crystallography. It is most likely that this "fluid region" allows the longer conjugated side to perform conformational changes around the *cis* C15═C15′, *trans* C13═C14, and *trans* C11═C12 bonds.

To reveal the intermolecular interactions, we tried to fit the models of ^{3}Car(I), ^{3}Car(R), and ^{3}Car(II) into the binding pocket of the RC. Here, we kept the structure of the shorter conjugated side as in the S_0 state and changed the conformation of the longer conjugated side according to the models. Only the peripheral part of the longer conjugated side is truncated and shown as a ball in Figure 5. The figure shows that the (0°, 0°, 0°) model of ^{3}Car(I) can be comfortably accommodated in the binding pocket. On the other hand, in the (+20°, −20°, +20°) and (+45°, −40°, +40°) models of ^{3}Car(R) and ^{3}Car(II), the longer conjugated side causes serious collision with the side chain of Phe M67 on the surface of the binding pocket (shown in magenta). However, we found that the fitting to the binding pocket becomes feasible when the Phe M67 side chain changes its conformation.

(b) Simulation of Conformational Changes of ^{3}Car in the Binding Pocket. Figure 5b shows conformational models in the longer conjugated side and the Phe M67 side chain in the binding pocket. *(i) Conformational Change from ^{3}Car-(I) to ^{3}Car(R).* First, the rotational motion around the C15═C15′ bond can be triggered by the intrinsic property of a 15-*cis* Car upon triplet excitation, i.e., the rapid isomerization around the C15═C15′ bond toward all-*trans*. When the

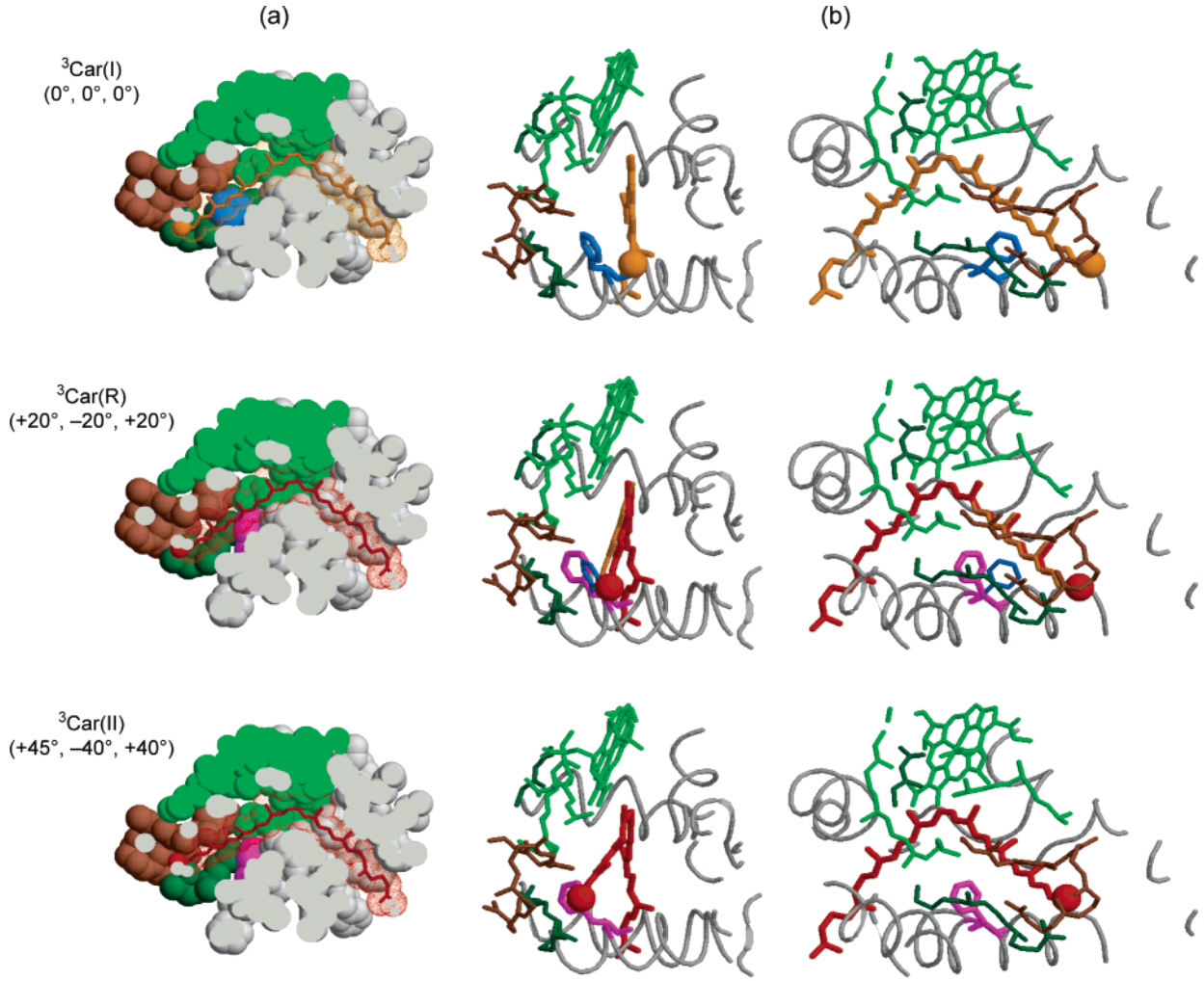

FIGURE 5: (a) Fitting of the models for ^{3}Car(I), ^{3}Car(R), and ^{3}Car(II) with torsional angles (0°, 0°, 0°), (+20°, −20°, +20°), and (+45°, −40°, +40°), around the *cis* C15═C15′, *trans* C13═C14, and *trans* C11═C12 bonds, respectively, to the Car binding pocket of the RC from *Rba. sphaeroides* Y determined by X-ray crystallography (*27*). (b) Imaginary picture of the conformational changes of the longer conjugated side of ^{3}Car in the binding pocket, shown in different colors including the peptide backbone (gray), B_M and H_M (light green and dark green), and Q_B (brown). The conformations of the conjugated chain of Car and the side chain of Phe M67 are shown in yellow and blue before collision and orange and magenta after collision. See the text for the details. The figure was drawn by the use of RASMOL (*29*).

torsional angle around the *cis* C15═C15′ bond reaches ∼20° in ^{3}Car(R), severe collision takes place between the longer conjugated side (shown in yellow) and the Phe M67 side chain (blue). Then, the most probable structural changes to avoid this collision include the shift of the Car-conjugated chain, by changing the pair of torsional angles around the *trans* C13═C14 and *trans* C11═C12 bonds toward the opposite direction, i.e., from (0°, 0°) to (−20°, +20°) (shown in orange), and the rotation of the Phe side chain by 74° (magenta). The small barrier in the ^{3}Car(I) → ^{3}Car(II) transformation (∼15 cm^{-1}) that we have observed may reflect the collision between the conjugated chain of Car and the side chain of Phe M67. *(ii) Conformational Change from ^{3}Car(R) to ^{3}Car(II).* When the rotations around the *cis* C15═C15′ bond and the *trans* C13═C14 and C11═C12 bonds continue further, the close contact of the longer conjugated side with the Q_B and H_M side chains blocks further rotation (>45°) around the *cis* C15═C15′ bond. Here again, the shift of the conjugated plane (see Figure 3, on the left-hand side) plays a most important role in releasing the strong steric interaction with the Phe M67 side chain.

Thus, the rotational motion around those *trans* double bonds can be rationalized in terms of the steric interaction, because the all-*trans* to *cis* isomerization never takes place via the T_1 state of free spheroidene in solution. The collision between the Car-conjugated chain and the Phe M67 side chain also rationalizes the incorporation of ^{3}Car(R) as an intermediate in the transformation from ^{3}Car(I) to ^{3}Car(II).

Evidence for the Hypothetical Mechanism of Triplet-Energy Dissipation. On the basis of a pair of observations, i.e., the rapid isomerization toward all-*trans* as the intrinsic T_1-state property of 15-*cis*-spheroidene in solution and the conformational changes of the RC-bound 15-*cis*-spheroidene from a flat to a substantially twisted conformation detected by resonance Raman spectroscopy, we *previously* proposed the following hypothetical mechanism of triplet-energy dissipation (*12*, *15*, *16*): "The rotational motions around the central double bonds cause a change in the orbital angular momentum and, as a result, a change in the spin angular momentum through the spin−orbit coupling, which facilitates the T_1 → S_0 relaxation accompanying the triplet-energy dissipation."

In the present investigation, we have tried to obtain evidence for this hypothetical mechanism. We have addressed three specific questions as described at the end of the Introduction, and now, we have obtained positive answers:

Question (1), Can the conformational change in the T_1 state be evidenced? We have discovered the transformation of ^{3}Car(I) → ^{3}Car(II) and, most likely, those of ^{3}Car(I) → ^{3}Car(R) → ^{3}Car(II) by the SVD and global-fitting analysis of time-resolved EPR spectra. Calculations of the zero-field splitting parameters, $|D|$ and $|E|$, suggested that the conformational changes take place in the order, (0°, 0°, 0°) → (+20°, −20°, +20°) → (+45°, −40°, +40°), around the *cis* C15═C15′, *trans* C13═C14, and *trans* C11═C12 bonds. The barrier to the ^{3}Car(I) → ^{3}Car(II) transformation was determined to be as low as ∼15 cm^{-1}. All proposed conformations can be nicely accommodated in the Car binding pocket of the RC determined by X-ray crystallography (*27*), when the rotation of the Phe M67 side chain and the shift of the Car-conjugated chain are taken into account.

Question (2), Can the T_1 → S_0 intersystem crossing, which dissipates the triplet energy and population, be correlated with the conformational change? We have found a leakage of the triplet population, during the process of the ^{3}Car(I) → ^{3}Car(II) transformation. Presumably, ^{3}Car(R) can be a representative intermediate generated by the collision of the Car-conjugated chain with the Phe M67 side chain.

Question (3), Can a sign of change in the spin angular momentum be detected during the conformational change? The change was identified as unique time-dependent changes in the spin polarization along the *z* axis, i.e., the rapid decay and the inversion of spin polarization. The direction and timing of the change strongly support the idea that the rotational motion around the central double bonds triggers the change in the orbital angular momentum and, as a result, the change in the spin angular momentum.

The results of the present investigation are in line with the hypothetical mechanism of triplet-energy dissipation that we proposed previously (*12*, *15*, *16*): the rotation around the central double bonds is evidenced; the leakage channel of the triplet population is identified; and the change in the spin angular momentum is shown. This mechanism should be investigated further by time-resolved absorption and Raman spectroscopies and, eventually, by time-resolved X-ray crystallography. The mechanism, by which the rotational motion around the central double bonds causes a change in the orbital angular momentum, should be investigated theoretically.

SUPPORTING INFORMATION AVAILABLE

Details of sample preparation and EPR spectroscopy, calculation of the zero-field splitting parameters, and simulation of the spectral patterns in the Materials and Methods; the reason why different triplet species were not identified in the previous investigations, determination of barriers for the transformation of ^{3}P → ^{3}Car(I) → ^{3}Car(II) → (with Figure S1), determination of the zero-field splitting parameters (Figure S2), the procedure and evaluation of the four-component, SVD and global-fitting analysis (Figure S3), determination of time-dependent changes in the spin polarization around the *x*, *y*, and *z* axes, evaluation of the results by reconstitution of time-resolved spectra by the use of relevant parameters (Figures S4−S6), a test analysis assuming no changes in the zero-field splitting parameters, $|D|$ and $|E|$, and no inversion of spin polarization (Figures S7−S9) in the Results; and X-ray structure of RC-bound spheroidene (Figure S10) and preliminary results in the time-resolved EPR spectroscopy of the LH2 complex from *Rba. sphaeroides* 2.4.1 in the Discussion. This material is available free of charge via the Internet at http://pubs.acs.org.

REFERENCES

1. Frank, H. A., and Cogdell, R. J. (1993) The photochemistry and function of carotenoids in photosynthesis, in *Carotenoids in Photosynthesis* (Young, A., and Britton, G., Eds.) pp 252−326, Chapman and Hall, London, U.K.
2. Lutz, M., Kleo, J., and Reiss-Husson, F. (1976) Resonance Raman scattering of bacteriochlorophyll, bacteriopheophytin and spheroidene in reaction centers of *Rhodopseudomonas spheroides*, *Biochem. Biophys. Res. Commun. 69*, 711−717.
3. Koyama, Y., Kito, M., Takii, T., Saiki, K., Tsukida, K., and Yamashita, J. (1982) Configuration of the carotenoid in the reaction centers of photosynthetic bacteria. Comparison of the resonance Raman spectrum of the reaction center of *Rhodopseudomonas sphaeroides* G1C with those of *cis*−*trans* isomers of *β*-carotene, *Biochim. Biophys. Acta 680*, 109−118.
4. Koyama, Y., Takii, T., Saiki, K., and Tsukida, K. (1983) Configuration of the carotenoid in the reaction centers of photosynthetic bacteria. (2) Comparison of the resonance Raman lines of the reaction centers with those of the 14 different *cis*−*trans* isomers of *β*-carotene, *Photobiochem. Photobiophys. 5*, 139−150.
5. Koyama, Y. (1991) Structures and functions of carotenoids in photosynthetic systems, *J. Photochem. Photobiol. B: Biol. 9*, 265−280.
6. Lutz, M., Szponarski, W., Berger, G., Robert, B., and Neumann, J.-M. (1987) The stereoisomerism of bacterial, reaction-center-bound carotenoids revisited: An electronic absorption, resonance Raman and ^{1}H-NMR study, *Biochim. Biophys. Acta 894*, 423−433.
7. Koyama, Y., Kanaji, M., and Shimamura, T. (1988) Configurations of neurosporene isomers isolated from the reaction center and the light-harvesting complex of *Rhodobacter sphaeroides* G1C. A resonance Raman, electronic absorption, and ^{1}H-NMR study, *Photochem. Photobiol. 48*, 107−114.
8. Koyama, Y., Takatsuka, I., Kanaji, M., Tomimoto, K., Kito, M., Shimamura, T., Yamashita, J., Saiki, K., and Tsukida, K. (1990) Configurations of carotenoids in the reaction center and the light-harvesting complex of *Rhodospirillum rubrum*. Natural selection of carotenoid configurations by pigment protein complexes, *Photochem. Photobiol. 51*, 119−128.
9. Hashimoto, H., and Koyama, Y. (1988) Time-resolved resonance Raman spectroscopy of triplet *β*-carotene produced from all-*trans*, 7-*cis*, 9-*cis*, 13-*cis*, and 15-*cis* isomers and high-pressure liquid chromatography analyses of photoisomerization via the triplet state, *J. Phys. Chem. 92*, 2101−2108.
10. Hashimoto, H., Koyama, Y., Ichimura, K., and Kobayashi, T. (1989) Time-resolved absorption spectroscopy of the triplet state produced from the all-*trans*, 7-*cis*, 9-*cis*, 13-*cis*, and 15-*cis* isomers of *β*-carotene, *Chem. Phys. Lett. 162*, 517−522.
11. Kuki, M., Koyama, Y., and Nagae, H. (1991) Triplet-sensitized and thermal isomerization of all-*trans*, 7-*cis*, 9-*cis*, 13-*cis*, and 15-*cis* isomers of *β*-carotene: Configurational dependence of the quantum yield of isomerization via the T_1 state, *J. Phys. Chem. 95*, 7171−7180.
12. Fujii, R., Furuichi, K., Zhang, J.-P., Nagae, H., Hashimoto, H., and Koyama, Y. (2002) *Cis*-to-*trans* isomerization of spheroidene in the triplet state as detected by time-resolved absorption spectroscopy, *J. Phys. Chem. A 106*, 2410−2421.
13. Koyama, Y., and Mukai, Y. (1993) Excited states of retinoids, carotenoids and chlorophylls as revealed by time-resolved, electronic absorption and resonance Raman spectroscopy, in *Biomolecular Spectroscopy Part B* (Clark, R. J. H., and Hester, R. E., Eds.) pp 49−137, John Wiley and Sons, Chichester, U.K.

14. Lutz, M., Chinsky, L., and Turpin, P.-Y. (1982) Triplet states of carotenoids bound to reaction centers of photosynthetic bacteria: Time-resolved resonance Raman spectroscopy, *Photochem. Photobiol. 36*, 503−515.
15. Ohashi, N., Ko-chi, N., Kuki, M., Shimamura, T., Cogdell, R. J., and Koyama, Y. (1996) The structures of S_0 spheroidene in the light-harvesting (LH2) complex and S_0 and T_1 spheroidene in the reaction center of *Rhodobacter sphaeroides* 2.4.1 as revealed by Raman spectroscopy, *Biospectroscopy 2*, 59−69.
16. Mukai-Kuroda, Y., Fujii, R., Ko-chi, N., Sashima, T., Koyama, Y., Abe, M., Gebhard, R., van der Hoef, I., and Lugtenburg, J. (2002) Changes in molecular structure upon triplet excitation of all-*trans*-spheroidene in *n*-hexane solution and 15-*cis*-spheroidene bound to the photo-reaction center from *Rhodobacter sphaeroides* as revealed by resonance-Raman spectroscopy and normal-coordinate analysis, *J. Phys. Chem. A 106*, 3566−3579.
17. McGann, W. J., and Frank, H. A. (1985) Transient electron spin resonance spectroscopy of the carotenoid triplet state in *Rhodopseudomonas sphaeroides* wild type, *Chem. Phys. Lett. 121*, 253−261.
18. Borovykh, I. V., Klenina, I. B., Proskuryakov, I. I., Gast, P., and Hoff, A. J. (2002) Magnetophotoselection study of the carotenoid triplet state in *Rhodobacter sphaeroides* reaction centers, *J. Phys. Chem. B 106*, 4305−4312.
19. Kim, S. S., and Weissman, S. I. (1976) Detection of transient electron paramagnetic resonance, *J. Magn. Reson. 24*, 167−169.
20. Torrey, H. C. (1949) Transient nutations in nuclear magnetic resonance, *Phys. Rev. 76*, 1059−1068.
21. Chen, W.-G., and Braiman, M. S. (1991) Kinetic analysis of time-resolved infrared difference spectra of the L and M intermediates of bacteriorhodopsin, *Photochem. Photobiol. 54*, 905−910.
22. Henry, E. R., and Hofrichter, J. (1992) Singular value decomposition: Application to analysis of experimental data, *Methods Enzymol. 210*, 129−192.
23. Yamaguchi, S., and Hamaguchi, H. (1998) Femtosecond ultraviolet−visible absorption study of all-*trans* → 13-*cis*•9-*cis* photoisomerization of retinal, *J. Chem. Phys. 109*, 1397−1408.
24. Borovykh, I. V., Proskuryakov, I. I., Klenina, I. B., Gast, P., and Hoff, A. J. (2000) Magnetophotoselection study of the lowest excited triplet state of the primary donor in photosynthetic bacteria, *J. Phys. Chem. B 104*, 4222−4228.
25. Frank, H. A., Chynwat, V., Posteraro, A., Hartwich, G., Simonin, I., and Scheer, H. (1996) Triplet state energy transfer between the primary donor and the carotenoid in *Rhodobacter sphaeroides* R-26.1 reaction centers exchanged with modified bacteriochlorophyll pigments and reconstituted with spheroidene, *Photochem. Photobiol. 64*, 823−831.
26. Angerhofer, A., Bornhäuser, F., Aust, V., Hartwich, G., and Scheer, H. (1998) Triplet energy transfer in bacterial photosynthetic reaction centres, *Biochim. Biophys. Acta 1365*, 404−420.
27. Arnoux, B., Gaucher, J.-F., Ducruix, A., and Reiss-Husson, F. (1995) Structure of the photochemical reaction centre of a spheroidene-containing purple bacterium, *Rhodobacter sphaeroides* Y, at 3 Å resolution, *Acta Crystallogr., Sect. D: Biol. Crystallogr. 51*, 368−379.
28. Thurnauer, M. C., Katz, J. J., and Norris, J. R. (1975) The triplet state in bacterial photosynthesis: Possible mechanisms of the primary photo-act, *Proc. Natl. Acad. Sci. U.S.A. 72*, 3270−3274.
29. Sayle, R. A., and Milner-White, E. J. (1995) RASMOL: Biomolecular graphics for all, *Trends Biochem. Sci. 20*, 374−376.

BI0511538